The CRISPR Journal
Volume 1, Number 4, 2018

DOI: 10.1089/crispr.2018.0018

The CRISPR Journal

RESEARCH ARTICLE

CRISPR-Based Editing Reveals Edge-Specific Effects in Biological Networks

Yi Li,[1,2] Chance M. Nowak,[2,3] Daniel Withers,[1,2] Alexander Pertsemlidis,[4] and Leonidas Bleris[1–3]

Abstract

Unraveling the properties of biological networks is central to understanding both normal and disease cellular phenotypes. Networks consist of functional elements (nodes) that form a variety of diverse connections (edges), with each node being a hub for multiple edges. Herein, in contrast to node-centric network perturbation and analysis approaches, we present a high-throughput CRISPR-based methodology for delineating the role of network edges. Ablation of network edges using a library targeting 93 miRNA target sites in 71 genes reveals numerous edges that control, with variable importance, cellular growth and survival under stress. To compare the impact of removing nodes versus edges in a biological network, we dissect a specific p53-microRNA pathway. We show that removal of the miR-34a target site from the anti-apoptotic gene *BCL2* desensitizes the cell to ectopic delivery of miR-34a in a p53-dependent manner. In summary, we demonstrate that network edges are critical to the function and stability of biological networks. Our results introduce a novel genetic screening opportunity via edge ablation and highlight a new dimension in biological network analysis.

Introduction

We focus on the network formed by p53 and its upstream and downstream regulators, which is critical to cell health yet incompletely understood. Since its discovery in 1979,[1] p53 has been shown to play a crucial role in maintaining genomic stability,[2] with >50% of human cancers harboring mutant or deleted p53.[3] Under normal conditions, the p53 protein exists in a latent form and at low concentration, but in response to various cellular stress signals such as DNA damage, hypoxia, and oncogene expression, post-translational modification of p53 results in its stabilization and accumulation.[4] As most human malignancies shut down the p53 tumor-suppressing responses, p53 is one of the critical targets for drug interventions in cancer therapy.[5,6]

A class of post-transcriptional regulators, called microRNAs (miRNAs), is directly associated with p53, either regulating the mRNA responsible for p53 production or being regulated by p53 and its partners.[7,8] miRNAs, in their mature forms, are small non-coding RNAs approximately 22 nucleotides in length that act as major regulators of gene expression. Since miRNAs are involved in critical cellular and physiological processes such as growth, differentiation, apoptosis, and metastasis, the gain or loss of critical miRNAs in a given cell type can have significant implications for cell fate.[9–12] Studies have revealed extensive crosstalk between the p53 network and miRNAs, but the specifics of how miRNAs participate in the regulation of p53 signaling and what they contribute to the role of p53 as a tumor suppressor remain largely elusive.

In miRNA-based networks, the edges are regulatory interactions between miRNAs and target mRNAs. These interactions are mediated by sequence complementarity and therefore are susceptible to genetic variation in either the miRNA or the target site—the seed sequence of the miRNA and the complementary region in the target site are considered the largest determinants of the interaction. Variation in miRNA binding sites has been associated with numerous diseases, including Tourette syndrome,[13] rheumatoid arthritis,[14] lupus,[15] psoriasis,[16] Crohn's disease,[17,18] Parkinson's disease,[19] hypertension,[20,21] diabetes and obesity,[22,23] and multiple cancers.[24–28] In the context of p53 signaling,[29] miR-34a regulates HDM4, a strong repressor of p53, creating a positive feedback loop in which high levels of miR-34a

[1]Department of Bioengineering, [2]Center for Systems Biology, and [3]Department of Biological Sciences, The University of Texas at Dallas, Richardson, Texas; and [4]Greehey Children's Cancer Research Institute, The University of Texas Health Science Center at San Antonio, San Antonio, Texas.

Address correspondence to: *Leonidas Bleris, The University of Texas at Dallas, NSERL 4.708, 800 West Campbell Road, Richardson, TX 75080,* E-mail: bleris@utdallas.edu

de-repress p53, which in turn transcriptionally upregulates the expression of miR-34a.

Network edges (e.g., miRNA–gene target interactions) are central to the function and stability of biological pathways. Today, we have the unprecedented opportunity to dissect individual cells and pathways with single-nucleotide specificity using genome editing. The most widely adopted editing methodology to date is the bacterial type II CRISPR* system, consisting of the CRISPR-associated protein Cas9 derived from *Streptococcus pyogenes* (SpCas9), a DNA endonuclease, and a guide RNA, which directs the binding of Cas9 to a DNA target upstream of a protospacer adjacent motif (PAM). The CRISPR technology has revolutionized our ability to probe and edit the human genome *in vitro* and *in vivo* through targeted gene disruption, insertion, deletion, single-nucleotide mutation, and chromosomal rearrangement.[30–32] Furthermore, pooled sgRNA libraries can be used for versatile *in vitro* screening to investigate phenotypes of interest. Recent examples include screens identifying genes conferring drug resistance,[33] genes involved in metastasis,[34] and long non-coding RNAs (lncRNAs) regulating human cancer cell growth.[35] Thus far, pooled sgRNA libraries have been applied to transcribed loci, which correspond to network *nodes*. Here, we selectively remove *edges* in the miRNA-p53 network, using a first-of-a-kind CRISPR-based screen. We demonstrate that removing edges sheds new light on pathways, in ways not achievable through node-based approaches, which may lead to novel and non-obvious therapeutic opportunities.

Materials and Methods

Preparation of the CRISPR plasmid library

The CRISPR plasmid library was prepared by following the lentiCRISPRv2 cloning protocol provided by Dr. Feng Zhang (Department of Biology, MIT, Cambridge, MA). Briefly, for each identified sgRNA target (20 nt), two oligos were synthesized. The first oligo was designed as 5′-CACCG-(20 nt sgRNA target sequence)-3′. The second oligo was designed as 5′-AAAC-(20 nt reverse complement of the sgRNA target sequence)-C-3′. All 93 pairs of oligonucleotides were synthesized by Sigma–Aldrich using its customized 96-well plate format (Supplementary Table S1; Supplementary Data are available online at www.liebertpub.com/crispr). Each well contained the pair of oligos for a specific sgRNA target (100 nmol for each). The oligo pairs were reconstituted using 100 μL of dH_2O. For annealing the oligo pairs, 2 μL of each of the reconstituted oligo solutions was mixed with 2 μL of 10 × T4 DNA Ligase Buffer (New England Biolabs, cat. no. B0202S) and 16 μL of dH_2O. The mixtures were heated at 95°C for 4 min and then left at room temperature for 60 min. One microgram of the lentiCRISPRv2 plasmid (Addgene; cat. no. 52961) was digested with 1 μL of Esp3I (Thermo Fisher Scientific; cat. no. ER0451) at 37°C for 1 h and run out on 1% agarose gel. The 12 kb band was extracted using the QIAquick Gel Extraction Kit (Qiagen; cat. no. 28704). One microliter of each of the annealed oligo pairs was mixed with 9,904 μL of dH_2O. Subsequently, 1 μL of the oligo mixture was ligated with Esp3I-digested lenti-CRISPRv2 using T4 DNA Ligase (New England Biolabs; cat. no. M0202S). To prepare the library, XL10-Gold Ultracompetent cells (Agilent; cat. no. 200314) were transformed, and >300 individual clones were pooled. To confirm complexity, the library was subjected to Sanger sequencing (Genewiz) using primer P1 and analyzed using FinchTV (Geospiza).

Generation of the CRISPR lentiviral screen library

To generate the lentiviral vectors, HEK293T cells were grown to 50–70% confluence and then transfected with 3.3 μg of the CRISPR plasmid library, 3.3 μg of the pMD2-VSVG plasmid, and 3.3 μg of the psPAX2 plasmid using 20 mL of JetPRIME (Polyplus; cat. no. 114-01). Twenty-four hours later, the medium was removed and replenished with 5 mL of complete growth medium. In the next 3 days, the growth medium containing lentiviral vectors was harvested, and 5 mL of fresh complete growth medium was replenished. The final pooled 15 mL growth medium was centrifuged at 1,811 g for 15 min at 4°C to remove cell debris. The supernatant was filtered through a 0.45 μm filter, dispensed into 1–2 mL aliquots and stored at −80°C. Viral titers were determined using a quantitative polymerase chain reaction (qPCR) Lentivirus Titration Kit (ABMGood; cat. no. LV900) following the manufacturer's instructions. Briefly, 2 μL of viral stock was mixed with 18 μL of virus lysis buffer and incubated at room temperature for 3 min. This viral lysate, together with positive control (STD1), positive control (STD2), and negative control (NTC), were subjected to quantitative reverse transcription PCR (qRT-PCR). Finally, the titer of the viral stock was calculated based on the formula provided by the manufacturer and determined to be 2.07×10^7 IU/mL. To generate the LIB-WT and LIB-$p53^{-/-}$ stable cells, approximately 10 million cells were seeded onto a 10 cm Petri dish. Sixteen hours later, cells were transduced using the lentiviral vectors at a multiplicity of infection (MOI) of 0.3. Forty-eight hours post transduction, cells were treated with 0.5 μg/mL of puromycin (Thermo Fisher Scientific; cat. no. A1113802). Polyclonal stable cell line libraries were established after around 2 weeks of drug selection.

*Clustered Regularly Interspaced Short Palindromic Repeats.

Sanger amplicon sequencing

To confirm the complexity of the LIB-WT and LIB-p53$^{-/-}$ cell line libraries, total genomic DNA was isolated from LIB-WT and LIB-p53$^{-/-}$ cells using the DNeasy Blood & Tissue Kit (Qiagen; cat. no. 69504). The cDNA fragments harboring the sgRNA target sequences were PCR amplified by using approximately 100 ng of the genomic DNA and primers P2 and P3 (Supplementary Table S2). PCR conditions were one cycle of 30 s at 98°C, 40 cycles of 10 s at 98°C, 30 s at 60°C, and 30 s at 72°C. The 181 bp product was then subjected to direct Sanger sequencing using primer P2 and analyzed using FinchTV (Geospiza). To determine editing efficiency, total genomic DNA was isolated from BCL2tgt-WT and BCL2tgt-p53$^{-/-}$ cells using the DNeasy Blood & Tissue Kit. cDNA fragments harboring the miR-34a target site within the 3′-UTR of BCL2 were PCR amplified by using ~100 ng of genomic DNA and primers P8 and P9. The 191 bp product was then subjected to direct Sanger sequencing using primer P9 and analyzed using FinchTV (Geospiza).

Next-generation sequencing

To determine the relative abundance of the 93 sgRNA target sequences before and after the CRISPR screen, total genomic DNA was isolated from miR-34a-treated LIB-WT and LIB-p53$^{-/-}$ cells at days 0 and 6 using the DNeasy Blood & Tissue Kit. cDNA fragments harboring the sgRNA target sequences were PCR amplified by using approximately 100 ng of the genomic DNA and primers P10 and P11, which added the 5′-overhang adapter sequence (5′-TCGTCGGCAGCGTCAGATGTG TATAAGAGACAG-3′) and the 3′-overhang adapter sequence (5′-GTCTCGTGGGCTCGGAGATGTGTATAA GAGACAG-3′) for subsequent Illumina next-generation sequencing (NGS) amplicon sequencing, which was performed at the Genome Sequencing Facility (GSF) at The University of Texas Health Science Center at San Antonio. To determine the editing efficacies of the BCL2 targets in the BCL2tgt-WT and BCL2tgt-p53$^{-/-}$ cells, total genomic DNA was isolated using the DNeasy Blood & Tissue Kit. cDNA fragments harboring the miR-34a target site within the 3′-UTR of BCL2 gene were PCR amplified by using approximately 100 ng of the genomic DNA and primers P16 and P17, and subsequently subjected to Illumina NGS amplicon sequencing, with around two million reads generated for each sample. The relative abundances of all 93 sgRNA target sequences were calculated and represented as counts per million reads. Log-transformed values were used for presentation. For more detailed description of the NGS data analysis, refer to Supplementary Methods: Next generation sequencing data analysis.

Apoptosis assay

To determine the non-apoptotic cell population 72 h post transfection with 25 nM of miR-34a mimic, 1 mL of the original cell growth medium was transferred into a 15 mL conical tube. Cells were washed with 1 mL of phosphate-buffered saline (PBS) solution, which was also collected. Cells were trypsinized using 150 μL of trypsin-ethylenediaminetetraacetic acid (EDTA) for 5 min at 37°C. Subsequently, the trypsin-EDTA was neutralized using 2 mL of the original cell growth medium/PBS washing solution mixture. The cells were harvested by centrifugation at 160 g for 5 min. The cell pellet was then re-suspended in 1 mL of PBS solution and then subjected to centrifugation at 160 g for 5 min. Apoptosis was quantified using the Dead Cell Apoptosis Kit with annexin V Alexa Fluor™ 488 and propidium iodide (PI; Invitrogen; cat. no. V13241), following manufacturer's instructions. Briefly, the harvested cell pellets were re-suspended in 100 μL of 1× annexin-binding buffer before being stained with 1 μL of PI (100 μg/μL) and 5 μL of stock annexin V Alexa Fluor™ 488 conjugate for 15 min in the dark. Stained cells were then diluted with 400 μL of 1× annexin-binding buffer before subjected to flow cytometry. Excitation/emission wavelengths for the annexin V Alexa Fluor™ 488 conjugate are 495/519 nm; for PI, they are 533/617 nm.

Cell viability assay

Approximately 150,000 of the HEK293, Flp-In-293, FLP-EDIT1, and FLP-EDIT2 cells were seeded onto six-well plates in 2 mL of complete medium. FLP-EDIT1 and FLP-EDIT2 cells were maintained with 0.5 μg/mL of puromycin. All cells were treated with 100 μg/mL of zeocin. For each cell type, six wells were included so that one of the wells could be harvested and counted on each day (from day 1 to day 6 after seeding). Three independent experiments were performed. For live cell counting, the cell suspension was mixed with 0.4% trypan blue solution (Invitrogen; cat. no. 15250) at a 1:1 ratio (volume:volume). Unstained, live cells were then counted using a hemocytometer (Hausser Scientific; cat. no. UX-79001-00) under a light microscope.

qRT-PCR

For measurement of BCL2 mRNA levels, total RNA was extracted using the RNeasy Mini Kit (Qiagen; cat. no. 74104) 48 h post transfection. First-strand synthesis was performed using the QuantiTect Reverse Transcription Kit (Qiagen; cat. no. 205311). Quantitative PCR was performed using the KAPA SYBR FAST Universal qPCR Kit (KAPABiosystems; cat. no. KK4601), with GAPDH levels used for normalization. Quantitative analysis was

performed using the $2^{-\Delta\Delta Ct}$ method. Fold-change values are reported as means with standard deviations. Primers used for BCL2 were (P4) 5′-CATGCTGGGGCCGTAC AG-3′ and (P5) 5′-GAACCGGCACCTGCACAC-3′. Primers used for GAPDH were (P6) 5′-AATCCCATCAC CATCTTCCA-3′ and (P7) 5′-TGGACTCCACGACGTA CTCA-3′.

Results

CRISPR-based screen for microRNA target editing

We focus on five miRNAs—miR-34a, miR-145, miR-192, miR-194, and miR-215—which are known to be directly or indirectly regulated by p53, and play elaborate roles in the p53 pathway.[36–38] The target genes for each miRNA were compiled from miRTarBase.[39] We selected targets that have been experimentally validated by multiple methods, including luciferase reporter assay, Western blot, and qRT-PCR (Supplementary Tables S3–S7). For each of the target genes, the miRNA target sites within its 3′-UTR were determined using TargetScan.[40] In total, 93 miRNA target sites were identified across the 71 target genes. The miRNAs and the 71 target genes are the nodes of the derived network, while the experimentally verified and high-confidence predicted interactions between the nodes, including interactions between miRNAs and target genes and between target genes themselves, are the network edges (Fig. 1a). To selectively edit these edges, we employed SpCas9-mediated non-homologous end joining, which typically introduces short insertions or deletions (indels) near its cutting site, and designed sgRNAs in which a PAM is adjacent to the miRNA target seed sequence(s) in the 3′-UTR[9] (Supplementary Tables S3–S7).

Next, we constructed a pooled CRISPR sgRNA library, containing both SpCas9 and sgRNA expression cassettes.[41] Equimolar amounts of the 93 pairs of oligonucleotides were mixed and cloned into a lentiviral vector (lentiCRISPRv2). To confirm library complexity, we sequenced the resulting plasmid library. The resulting reads displayed consistent flanks with a 20 bp ''noisy'' sgRNA target sequence, matching the expected pattern from the sgRNA mixture (Supplementary Fig. S1). Subsequently, the lentiviral library was used to infect HCT116 wild-type (WT) and HCT116 $p53^{-/-}$ cells at a MOI of 0.3, which has been shown[42] to yield at most one integration of the sgRNA cassette in the majority of cells (Fig. 1b). To verify the complexity of our resulting libraries in cells (named LIB-WT and LIB-$p53^{-/-}$) was maintained, the sgRNA locations were amplified from genomic DNA and subjected to Sanger sequencing, which again displayed the expected pattern (Supplementary Fig. S2).

In parallel, to test the efficacy of the viral system, we prepared two CRISPR lentiviral vectors that target the open reading frame (ORF) of the zeocin resistance gene (target 1: 5′-TCGCCGGAGCGGTCGAGTTC-TGG; target 2: 5′-CTCACCGCGCGCGACGTCGC-CGG; PAM underlined), and stably integrated them into cell line Flp-In-293 (Thermo Fisher Scientific), which harbors the zeocin resistance gene. As shown in Supplementary Figure S3, disruption of the zeocin resistance gene abolished resistance to zeocin (100 μg/mL) in the two

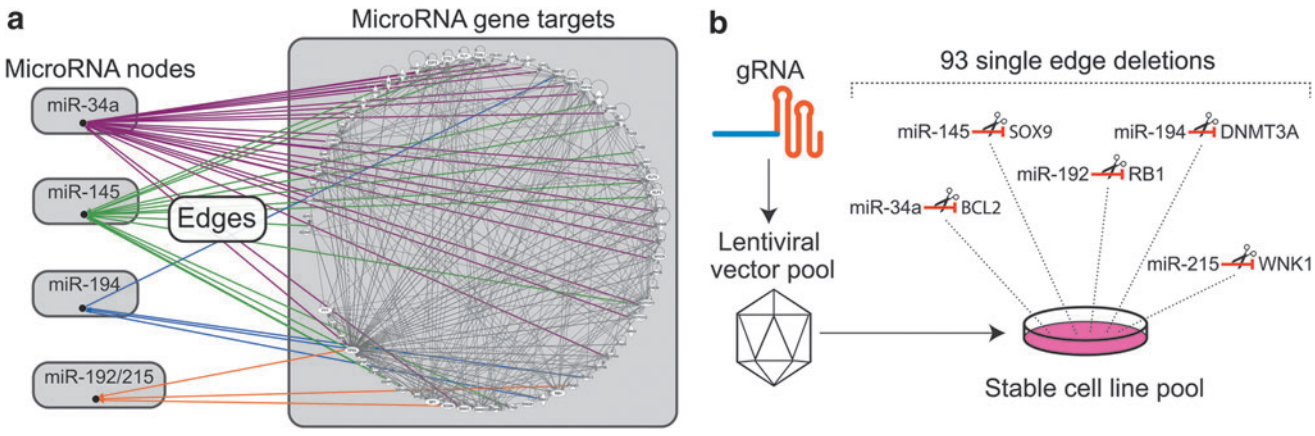

FIG. 1. p53-miRNA network and CRISPR-based edge screens. **(a)** Complexity of the p53-miRNA network with nodes comprising the indicated miRNAs and their 71 target genes (detailed list provided in Supplementary Tables S3–S7) and edges based on experimentally verified and high-confidence predicted direct interactions, derived using Qiagen Ingenuity Pathway Analysis. **(b)** CRISPR-based lentiviral libraries were prepared using the lentiCRISPRv2 system. The stably integrated CRISPR sgRNA constructs were recovered by PCR and the sgRNA targets were identified using NGS. Gene targets for each miRNA are listed in Supplementary Tables S3–S7.

resulting cell lines (FLP-EDIT1 and FLP-EDIT2) compared to the parental Flp-In-293 cells.

Using the established cell lines (LIB-WT and LIB-p53$^{-/-}$), we focused on the role of miR-34a in the overall p53-miRNA network (Fig. 1a). miR-34a is transcriptionally activated by p53 and induces an anti-proliferative phenotype including senescence, cell cycle arrest at the G1 phase, and apoptosis.[43,44] In turn, overexpression of miR-34a increases p53 protein level and stability.[36] Importantly, our established cell lines (LIB-WT and LIB-p53$^{-/-}$) do not produce miR-34a (Supplementary Fig. S4), and can therefore be considered to lack the miR-34a node. The miR-34a targets and target sites are still present, however, and therefore the addition of miR-34a to these cells re-establishes the miR-34a network. Compared to baseline miR-34a expression, there is a 71-fold increase in mature miR-34a levels 48 h post transfection.

We adopted a growth competition assay mediated by ectopic exposure to miR-34a mimics. miRNA mimics are chemically synthesized double-stranded RNA molecules that when transfected into a cell behave similar to a mature endogenous miRNA, regulating the same mRNA (and non-mRNA) targets through the same interactions as the endogenous miRNAs. We treated both cell lines (LIB-WT and LIB-p53$^{-/-}$) to 25 nM of miR-34a mimic for 6 days. Cells were harvested at day 0 (before miRNA mimic transfection) and at day 6. For each sample, sgRNA constructs were amplified from genomic DNA and subjected to NGS amplicon sequencing to assess the relative abundance for each of the 93 sgRNA target sequences (Supplementary Tables S8 and S9). The most enriched or depleted sgRNA targets, defined by fold changes between day 6 and day 0 > 10, were identified for both LIB-WT and LIB-p53$^{-/-}$ cells (Fig. 2 and Supplementary Table S10).

Intriguingly, *RBX1* (RING-box protein 1), a RING subunit of SCF (Skp1, Cullins, F-box) E3 ubiquitin ligases, was highly enriched in both cell lines. Although not a direct target of miR-34a, overexpression of *RBX1* has been demonstrated to increase cancer cell survival,[45] and thus could serve as a general response mechanism to cellular stress induced by ectopic miR-34a. Additionally, for a subset of gene targets, we observed differential response to miR-34a mimic between the LIB-WT and LIB-p53$^{-/-}$ cells (Supplementary Table S10). For example, the sgRNA targeting the anti-apoptotic gene BCL2 was enriched in the LIB-p53$^{-/-}$ cells after miR-34a mimic transfection, while no enrichment was observed in the LIB-WT cells (Supplementary Fig. S5).

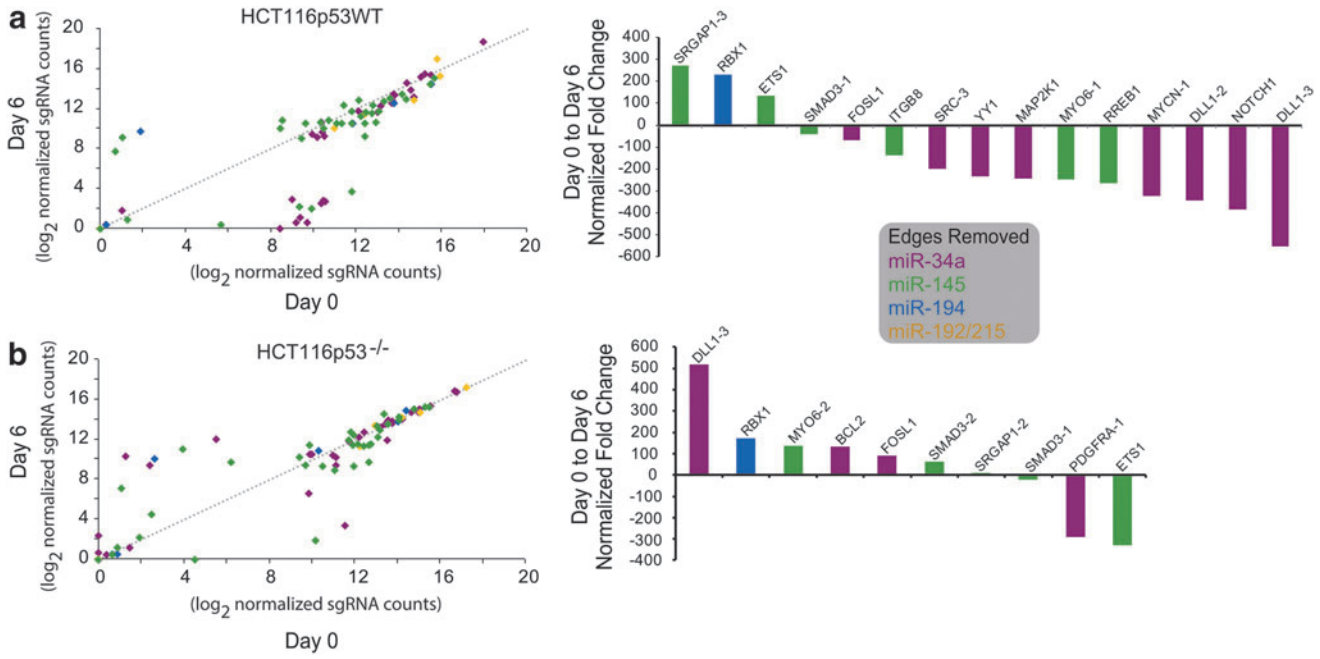

FIG. 2. High-throughput editing of edges with CRISPR libraries in **(a)** HCT116p53WT (LIB-WT) and **(b)** HCT116p53$^{-/-}$ (LIB-p53$^{-/-}$) cells. The sgRNA targets showing the highest fold changes (>10) after 6 days treatment of 25 nM with miR-34a mimic are shown, with positive values indicating enrichment and negative values indicating depletion.

Node perturbations versus edge edits in biological networks

Our edge editing approach (Fig. 2b) revealed several clones that are enriched or depleted after prolonged exposure to ectopic miR-34a. To assess the impact of edge removal (through ablation of miRNA–target interactions), we focused on *BCL2*, a gene that shows differential expression in response to miR-34a treatment between the two cell lines (Fig. 2b) and is known to be involved in cell survival.[46]

Returning to the HCT116 WT and HCT116 p53$^{-/-}$ cells, we removed the miR-34a target site from the *BCL2* locus. We prepared a single sgRNA construct designed against the BCL2 3′-UTR and established stable cell lines (BCL2tgt-WT and BCL2tgt-p53$^{-/-}$) using the same viral delivery system. Sanger and NGS sequencings of PCR products spanning the sgRNA target site showed that edits (indels) occurred immediately upstream of the PAM (Supplementary Figs. S6 and S7) in both cell lines. Additionally, we compared the sgRNA sequence targeting *BCL2* (5′-AATCAGCTATTTACTGCCAAA GG-3′; Supplementary Tables S3–S7) against the human genome, confirming *BCL2* as the unique target and indicating that nonspecific targeting by this sgRNA should be minimal.

Treating delivery of ectopic miR-34a mimic as perturbation of a network node and removal of the miR-34a/*BCL2* interaction as perturbation of a network edge (Fig. 3a), there are four possible combinations (node and edge present/absent). When miR-34a levels are low (i.e., the node is absent), the presence or absence of the edge does not impact survival (Supplementary Fig. S8) of either cell line.

In the context of node perturbation, the introduction of ectopic miR-34a in WT cells induces apoptosis (Fig. 3b, right panel, and Supplementary Fig. S9; cell viability is 87.6% without the miR-34a node, and 71.6% with the miR-34a node; $p = 0.006$). Similar changes were observed in p53$^{-/-}$ cells (Fig. 3b, left panel, and Supplementary Fig. S9; cell viability is 86.1% without the miR-34a

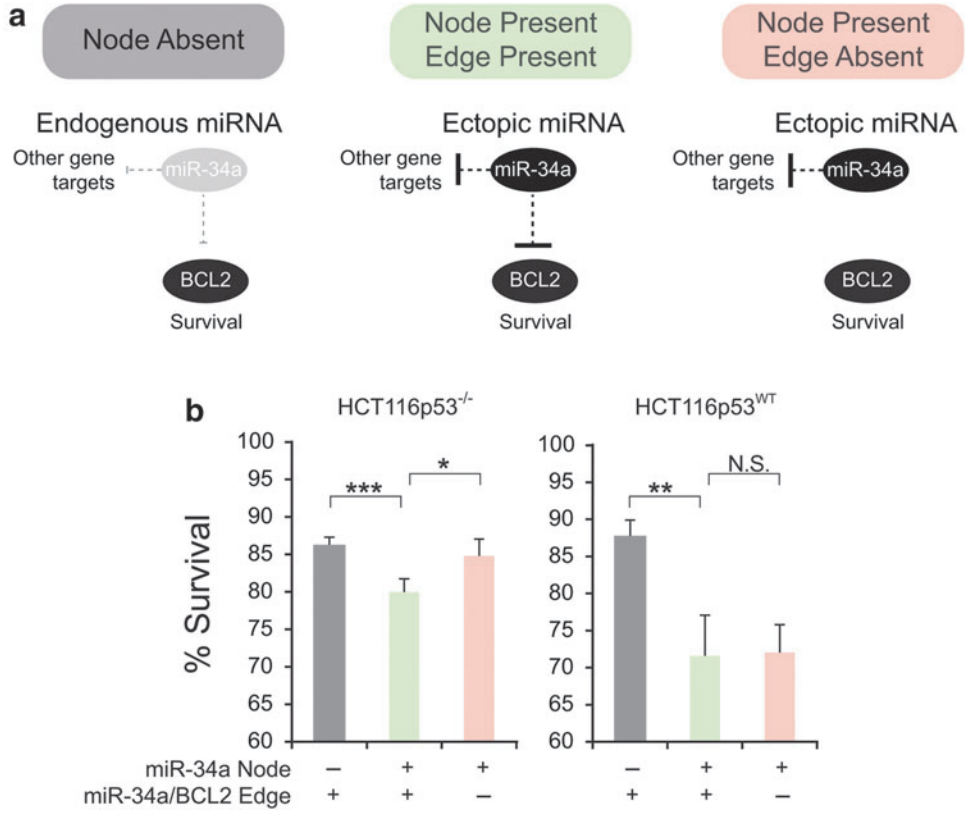

FIG. 3. Growth competition analysis after ectopic miR-34a delivery using node vs. edge approaches. **(a)** Schematic illustration of node versus edge analysis. Ectopic miR-34a represents a network node and the miR-34a/BCL2 interaction represents a network edge. **(b)** The node-based approach shows that addition of the miR-34a node induces apoptosis in both p53 WT and deficient cells. In contrast, the edge-based approach reveals that introduction of the miR-34a/BCL2 edge induces apoptosis only in the p53-deficient cells and not in p53-WT cells.

node, and 80.0% with the miR-34a node; $p=0.002$). In this case, perturbing the miR-34a node results in the same behavior for both p53 WT and p53$^{-/-}$ cells.

In the context of edge perturbation, the response of the cell lines to ectopic miR-34a is sensitive to the presence of the miR-34a/BCL2 edge. Specifically, removing the ability of miR-34a to regulate BCL2 in the p53$^{-/-}$ cells induces apoptosis (Fig. 3b, left panel, and Supplementary Fig. S9; cell viability is 84.8% without the miR-34a/BCL2 edge, and 80.0% with the miR-34a/BCL2 edge; $p=0.015$), while no such phenotypic changes are observed in p53 WT cells (Fig. 3b, right panel, and Supplementary Fig. S9; cell viability is 72.0% without the miR-34a/BCL2 edge, and 71.6% with the miR-34a/BCL2 edge; $p=0.900$). We note that the same conclusions can be drawn when quantifying the early or late apoptotic cells (Supplementary Fig. S10).

To explore the response to miR-34a in BCL2tgt-WT cells further, we quantified expression of the BCL2 mRNA in response to miR-34a mimics using qRT-PCR. As expected, miR-34a suppresses the expression of BCL2 mRNA in the WT and p53$^{-/-}$ cells by 55% and 40%, respectively (Supplementary Fig. S11). In the BCL2tgt-p53$^{-/-}$ cells, ectopic miR-34a has a minimal effect on BCL2 mRNA level (95% compared to the control-treated sample; $p=0.71$). In the BCL2tgt-WT cells, ectopic miR-34a results in a significant downregulation of BCL2 expression (62% compared to the control-treated sample; $p=0.028$), possibly due to additional p53-miR-34a regulatory mechanisms.

Discussion

Biological networks consist of nodes and the interactions between them (edges). Conventional screening methods remove one node at a time, disrupting all edges connected to that node and therefore producing a relatively blunt effect. An inhibitor that perturbs or removes a single node yields diverse and systemic changes in the whole network through both direct and indirect connections,[47] which may explain the heterogeneity observed with single molecule associated therapeutics.

Our approach reveals edge-specific effects related to the pro-apoptotic p53 and anti-apoptotic Bcl-2 proteins, focal nodes of apoptotic signaling. Normally, p53-dependent inhibition of Bcl-2 and induction of BAX, PUMA, and NOXA overcome the anti-apoptotic threshold set by Bcl-2 family members. Conceivably, the difference in apoptosis observed between the BCL2tgt-WT and BCL2tgt-p53$^{-/-}$ cells treated with miR-34a mimics (Fig. 3b) may be explained by the presence of WT p53-dependent upregulation of PUMA or NOXA in p53 WT cells and not in p53$^{-/-}$ cells. Additionally, p53 could disrupt the binding of POU4F1 (POU Class 4 Homeobox 1) to the promoter of BCL2 and thus indirectly downregulate BCL2 expression (Supplementary Fig. S11).

Taken together, our results show that the disruption of the network edge between miR-34a and BCL2 can revert the miR-34a-dependent triggered apoptotic effects in a p53-deficient cell model. In WT cells, introducing miR-34a presumably indirectly triggers the suppression of the expression of Bcl-2 via an alternative p53-related pathway, leading to increased apoptosis.

In conclusion, our CRISPR-mediated edge screening can be used to dissect critical biological interactions essential to cell growth and survival. More generally, we demonstrate that the subtle effect of our edge removal methodology offers superior resolution and granularity in the analysis of biological networks and can lead to the identification of previously hidden interactions and opportunities for intervention.

Acknowledgments

This work was funded by the U.S. National Science Foundation (NSF) CAREER grant 1351354, NSF 1361355, and the University of Texas at Dallas. We thank S. Lawson for technical support.

Author Disclosure Statement

The authors declare no competing financial interests.

References

1. DeLeo AB, Jay G, Appella E, et al. Detection of a transformation-related antigen in chemically induced sarcomas and other transformed cells of the mouse. *Proc Natl Acad Sci U S A* 1979;76:2420–2424.
2. Vousden KH, Prives C. Blinded by the light: the growing complexity of p53. *Cell* 2009;137:413–431. DOI: 10.1016/j.cell.2009.04.037.
3. Levine AJ. p53, the cellular gatekeeper for growth and division. *Cell* 1997;88:323–331.
4. Batchelor E, Loewer A, Lahav G. The ups and downs of p53: understanding protein dynamics in single cells. *Nat Rev Cancer* 2009;9:371–377. DOI: 10.1038/nrc2604.
5. Parrales A, Iwakuma T. Targeting oncogenic mutant p53 for cancer therapy. *Front Oncol* 2015;5:288. DOI: 10.3389/fonc.2015.00288.
6. Hong B, van den Heuvel APJ, Prabhu VV, et al. Targeting tumor suppressor p53 for cancer therapy: strategies, challenges and opportunities. *Curr Drug Targets* 2014;15:80–89.
7. He L, He X, Lim LP, et al. A microRNA component of the p53 tumour suppressor network. *Nature* 2007;447:1130–1134. DOI: 10.1038/nature05939.
8. Tarasov V, Jung P, Verdoodt B, et al. Differential regulation of microRNAs by p53 revealed by massively parallel sequencing: miR-34a is a p53 target that induces apoptosis and G(1)-arrest. *Cell Cycle* 2007;6:1586–1593. DOI: 10.4161/cc.6.13.4436.
9. Bartel DP. MicroRNAs: target recognition and regulatory functions. *Cell* 2009;136:215–233. DOI: 10.1016/j.cell.2009.01.002.
10. Filipowicz W, Bhattacharyya SN, Sonenberg N. Mechanisms of post-transcriptional regulation by microRNAs: are the answers in sight? *Nat Rev Genet* 2008;9:102–114. DOI: 10.1038/nrg2290.

11. Moore R, Ooi HKHK, Kang T, et al. MiR-192-mediated positive feedback loop controls the robustness of stress-induced p53 oscillations in breast cancer cells. *PLoS Comput Biol* 2015;11:e1004653. DOI: 10.1371/journal.pcbi.1004653.
12. Lee J, Lee J, Farquhar KS, et al. Network of mutually repressive metastasis regulators can promote cell heterogeneity and metastatic transitions. *Proc Natl Acad Sci U S A* 2014;111:E364–E373. DOI: 10.1073/pnas.1304840111.
13. Abelson JF, Kwan KY, O'Roak BJ, et al. Sequence variants in SLITRK1 are associated with Tourette's syndrome. *Science* 2005;310:317–320. DOI: 10.1126/science.1116502.
14. Chatzikyriakidou A, Voulgari PV, Georgiou I, et al. A polymorphism in the 3′-UTR of interleukin-1 receptor-associated kinase (IRAK1), a target gene of miR-146a, is associated with rheumatoid arthritis susceptibility. *Joint Bone Spine* 2010;77:411–413. DOI: 10.1016/jbspin.2010.05.013.
15. Consiglio CR, Veit TD, Monticielo OA, et al. Association of the HLA-G gene +3142C>G polymorphism with systemic lupus erythematosus. *Tissue Antigens* 2011;77:540–545. DOI: 10.1111/j.1399-0039.2011.01635.x.
16. Wu L-S, Li FF, Sun LD, et al. A miRNA-492 binding-site polymorphism in BSG (basigin) confers risk to psoriasis in central south Chinese population. *Hum Genet* 2011;130:749–757. DOI: 10.1007/s00449-011.
17. Brest P, Lapaquette P, Souidi M, et al. A synonymous variant in IRGM alters a binding site for miR-196 and causes deregulation of IRGM-dependent xenophagy in Crohn's disease. *Nat Genet* 2011;43:242–245. DOI: 10.1038/ng.762.
18. Kulkarni S, Qi Y, O'Huigin C, et al. Genetic interplay between HLA-C and MIR148A in HIV control and Crohn disease. *Proc Natl Acad Sci U S A* 2013;110:20705–20710. DOI: 10.1073/pnas.1312237110.
19. Wang G, van der Walt JM, Mayhew G, et al. Variation in the miRNA-433 binding site of FGF20 confers risk for Parkinson disease by overexpression of alpha-synuclein. *Am J Hum Genet* 2008;82:283–289. DOI: 10.1016/j.ajhg.2007.09.021.
20. Sethupathy P, Borel C, Gagnebin M, et al. Human microRNA-155 on chromosome 21 differentially interacts with its polymorphic target in the AGTR1 3′ untranslated region: a mechanism for functional single-nucleotide polymorphisms related to phenotypes. *Am J Hum Genet* 2007;81:405–413. DOI: 10.1086/519979.
21. Hanin G, Shenhar-Tsarfaty S, Yayon N, et al. Competing targets of microRNA-608 affect anxiety and hypertension. *Hum Mol Genet* 2014;23:4569–4580. DOI: 10.1093/hmg/ddu170.
22. Lv K, Guo Y, Zhang Y, et al. Allele-specific targeting of hsa-miR-657 to human IGF2R creates a potential mechanism underlying the association of ACAA-insertion/deletion polymorphism with type 2 diabetes. *Biochem Biophys Res Commun* 2008;374:101–105. DOI: 10.1016/j.bbrc.2008.06.102.
23. Richardson K, Louie-Gao Q, Arnett DK, et al. The PLIN4 variant rs8887 modulates obesity related phenotypes in humans through creation of a novel miR-522 seed site. *PLoS One* 2011;6:e17944. DOI: 10.1371/journal.pone.0017944.
24. Ryan BM, Robles AI, McClary AC, et al. Identification of a functional SNP in the 3′UTR of CXCR2 that is associated with reduced risk of lung cancer. *Cancer Res* 2015;75:566–575. DOI: 10.1158/0008-5472.CAN-14-2101.
25. Chin LJ, Ratner E, Leng S, et al. A SNP in a let-7 microRNA complementary site in the KRAS 3′ untranslated region increases non–small cell lung cancer risk. *Cancer Res* 2008;68. DOI: 10.1158/0008-5472.CAN-08-2129.
26. Zu Y, Ban J, Xia Z, et al. Genetic variation in a miR-335 binding site in BIRC5 alters susceptibility to lung cancer in Chinese Han populations. *Biochem Biophys Res Commun* 2013;430:529–534. DOI: 10.1016/j.bbrc.2012.12.001.
27. Xiong F, Wu C, Chang J, et al. Genetic variation in an miRNA-1827 binding site in MYCL1 alters susceptibility to small-cell lung cancer. *Cancer Res* 2011;71:5175–5181. DOI: 10.1158/0008-5472.CAN-10-4407.
28. Pu X, Roth JA, Hildebrandt MA, et al. MicroRNA-related genetic variants associated with clinical outcomes in early-stage non-small cell lung cancer patients. *Cancer Res* 2013;73:1867–1875. DOI: 10.1158/00080-5472.CAN-12-0873.
29. Okada N, Lin C-P, Ribeiro MC, et al. A positive feedback between p53 and miR-34 miRNAs mediates tumor suppression. *Genes Dev* 2014;28:438–450. DOI: 10.1101/gad.233585.113.
30. Mali P, Yang L, Esvelt KM, et al. RNA-guided human genome engineering via Cas9. *Science* 2013;339:823–826. DOI: 10.1126/science.1232033.
31. Rong Z, Zhu S, Xu Y, et al. Homologous recombination in human embryonic stem cells using CRISPR/Cas9 nickase and a long DNA donor template. *Protein Cell* 2014;5:258–260. DOI: 10.1007/s13238-014-0032-5.
32. Li J-F, Aach J, Norville JE, et al. Multiplex and homologous recombination-mediated genome editing in Arabidopsis and *Nicotiana benthamiana* via guide RNA/Cas9. *Nat Biotechnol* 2013;31:688–691. DOI: 10.1038/nbt.2654.
33. Wang T, Wei JJ, Sabatini DM, et al. Genetic screens in human cells using the CRISPR-Cas9 system. *Science* 2014;343:80–84. DOI: 10.1126/science.1246981.
34. Chen S, Sanjana NE, Zheng K, et al. Genome-wide CRISPR screen in a mouse model of tumor growth and metastasis. *Cell* 2015;160:1246–1260. DOI: 10.1016/j.cell.2015.02.038.
35. Zhu S, Li W, Chen CH, et al. Genome-scale deletion screening of human long non-coding RNAs using a paired-guide RNA CRISPR-Cas9 library. *Nat Biotechnol* 2016;34:1279–1286. DOI: 10.1038/nbt.3715.
36. Navarro F, Lieberman J. miR-34 and p53: new insights into a complex functional relationship. *PLoS One* 2015;10:e0132767. DOI: 10.1371/journal.pone.0132767.
37. Sundaram P, Hultine S, Smith LM, et al. p53-responsive miR-194 inhibits thrombospondin-1 and promotes angiogenesis in colon cancers. *Cancer Res* 2011;71:7490–7501. DOI: 10.1158/0008-5472.CAN-11-1124.
38. Feng Z, Zhang C, Wu R, et al. Tumor suppressor p53 meets microRNAs. *J Mol Cell Biol* 2011;3:44–50. DOI: 10.1093/jmcb/mjq040.
39. Chou C-H, Chang NW, Shrestha S, et al. miRTarBase 2016: updates to the experimentally validated miRNA-target interactions database. *Nucleic Acids Res* 2016;44:D239–D247. DOI: 10.1093/nar/gkv1258.
40. Agarwal V, Bell GW, Nam J-W, et al. Predicting effective microRNA target sites in mammalian mRNAs. *Elife* 2015;4:e05005. DOI: 10.7554/eLife.05005.
41. Sanjana NE, Shalem O, Zhang F. Improved vectors and genome-wide libraries for CRISPR screening. *Nat Methods* 2014;11:783–784. DOI: 10.1038/nmeth.3047.
42. Shalem O, Sanjana NE, Hartenian E, et al. Genome-scale CRISPR-Cas9 knockout screening in human cells. *Science* 2014;343:84–87. DOI: 10.1126/science.1247005.
43. Chang T-C, Wentzel EA, Kent OA, et al. Transactivation of miR-34a by p53 broadly influences gene expression and promotes apoptosis. *Mol Cell* 2007;26:745–752. DOI: 10.1016/j.molcel.2007.05.010.
44. Bader AG. miR-34—a microRNA replacement therapy is headed to the clinic. *Front Genet* 2012;3:120. DOI: 10.1016/j.molcel.2007.05.010.
45. Jia L, Sun Y. RBX1/ROC1-SCF E3 ubiquitin ligase is required for mouse embryogenesis and cancer cell survival. *Cell Div* 2009;4:16. DOI: 10.1186/1747-1028-4-16.
46. Cory S, Adams JM. The Bcl-2 family: regulators of the cellular life-or-death switch. *Nat Rev Cancer* 2002;2:647–656. DOI: 10.1038/nrc883.
47. Kang T, Moore R, Li Y, et al. Discriminating direct and indirect connectivities in biological networks. *Proc Natl Acad Sci U S A* 2015;112:12893–12898.

Received for publication April 9, 2018;
Revised May 22, 2018;
Accepted July 17, 2018.